Journal of Physics: Conference Series **455** (2013) 012003 doi:10.1088/1742-6596/455/1/012003

Hadronic resonance production in pp and Pb–Pb collisions at LHC with the ALICE experiment

A. Badalá[1] and H. Oeschler[2] for the ALICE collaboration

[1] INFN-Sezione di Catania, V. S. Sofia 64, Catania, I95125, Italy
[2] Institut für Kernphysik, Technische Universität Darmstadt, Darmstadt, Germany

E-mail: Angela.Badala@ct.infn.it

Abstract. Resonances, with their lifetimes comparable to that of the fireball, can be used to estimate the time span and hadronic interaction cross section in the phase between chemical and kinetic freeze-out. In pp collisions, measurements of resonances provide an important baseline for heavy-ion data and allow for the tuning of QCD-inspired particle production models. The ALICE collaboration measured $K^*(892)^0$ and $\phi(1020)$ production, both in pp collisions at $\sqrt{s}$=7 TeV and in Pb–Pb collisions at $\sqrt{s_{NN}}$=2.76 TeV. The inelastic yield of $\Sigma(1385)^{\pm}$ in pp collision at $\sqrt{s}$=7 TeV was also measured. Transverse momentum spectra, ratios to stable particles and a comparison between central and peripheral production are shown.

1. Introduction

The study of resonance production plays an important role both in elementary and in heavy ion collisions. In pp and e^+e^- collisions, it contributes to the understanding of hadron production [1, 2] as the decay products of resonances represent a large fraction of the final state particles. In addition, it provides a reference for tuning event generators inspired by Quantum Chromodynamics (QCD) such as PHOJET [3] and PYTHIA [4]. Hadronic resonances are a sensitive probe of the dynamical evolution of the fireball. Due to their short lifetime (a few fm/c) a significant fraction decays during the evolution from chemical to kinetic freeze-out and their hadronic daughters interact with the medium during the fireball expansion [5, 6, 7, 8]. In particular, products of their hadronic decay may rescatter reducing the measured resonance signal. Resonances may also be regenerated through collisions of hadrons. The competition between resonance-generating processes and rescattering, and therefore the ratio of resonance yields to non-resonance yield is governed by the lifetime and the temperature of the hadronic medium. Thermal models [7, 9, 10, 11] predict particle ratios as function of the chemical freeze-out temperature (T_{ch}) and the time between chemical and thermal freeze-out. Particularly interesting is the comparison of ϕ and K^* production, considering the different lifetimes (about a factor 10) of the two resonances. Due to the large lifetime (44 fm/c) the ϕ is expected to decay outside the hot and dense interacting medium.

2. Experimental setup and data analysis

The results reported in this paper refer to analyses carried out using a sample of minimum-bias pp data at $\sqrt{s}$=7 TeV (60 to 250 millions events, for the different resonances analyzed) and

of minimum-bias Pb–Pb data at $\sqrt{s_{\rm NN}}$=2.76 TeV (about 10 millions events), collected during 2010. The events are selected with a primary vertex within 10 cm of the detector center.

2.1. Experimental setup

The ALICE detector [12, 13] provides extensive particle tracking and identification in the central pseudorapidity range ($|\eta| \leq 0.9$) as well as muon tracking and identification at forward angles ($-2.5 > \eta > -4$). For the analysis described in this paper, only the central barrel has been used. The central tracking and particle identification detectors include, from the innermost outwards, the Inner Tracking System (ITS), the Time Projection Chamber (TPC) and the Time of Flight array (TOF). The central detectors are embedded in a 0.5 T solenoidal field. The moderate field, together with a low material budget permits the reconstruction of low $p_{\rm T}$ tracks. Furthermore, two forward scintillator hodoscopes (VZERO) placed along the beam direction at -0.9 m and 3.3 m on either side of the interaction point, which cover the pseudorapidity regions $-3.7 < \eta < -1.7$ and $2.8 < \eta < 5.1$, were used for minimum-bias triggering and for rejecting beam-gas interactions.

The Inner Tracking System (ITS) is a silicon detector that surrounds the interaction point, with six layers between radii 3.9 cm to 43 cm from the beam axis. The two innermost layers, based on silicon pixels (SPD), are also used as an on-line trigger and to reconstruct the collision vertex with a resolution better than 100 μm.

The TPC [14] provides track reconstruction with up to 159 three-dimensional space points per track in a cylindrical active volume of about 90 m^3. The standard tracking used in this analysis combines the information from the ITS and TPC. The momentum resolution of the TPC is in the range 1-7% for pions with $1<p_{\rm T}<10$ GeV/c. Furthermore it provides very good resolution in the distance of closest approach to the vertex (impact parameter resolution in the transverse direction is <100 μm for $p_{\rm T}>1$ GeV/c) and hence an excellent separation of primary and secondary particles.

The TPC identifies particles via the specific energy loss dE/dx determined with a truncated-mean procedure. It achieves a resolution ranging from 5-6.5% (tracks with 159 clusters - mean over all the reconstructed tracks) in pp and Pb–Pb collisions. Identification is achieved by calculating the difference between the measured energy loss and the one expected for different mass hypotheses. A selection on this difference, normalized to the resolution $\sigma_{\rm TPC}$, is optimized for each analysis and depends in general on the signal to background ratio and on the transverse momentum. The TPC dE/dx measurements allow pions to be separated from kaons for momenta up to $p \sim$0.7 GeV/c, while the proton/antiproton band starts to overlap with the pion/kaon band at $p \sim$1 GeV/c. The electron/positron dE/dx crosses the other bands at various momenta.

In order to ensure high efficiency and good dE/dx resolution and to minimize the contamination from secondaries and fakes, tracks were required to have at least 70 reconstructed clusters in the TPC. To improve the resolution (<1% at $p_{\rm T}\sim$1 GeV/c), tracks were accepted only in the range $|\eta| < 0.8$ (i.e. well within the TPC acceptance) and with $p_{\rm T}\geq 0.15$ GeV/c.

The Time-of-Flight Detector (TOF) is an array of multi-gap resistive-plate chambers placed at a radius of 370 to 399 cm. Particles are identified by the difference between the measured time-of-flight and the one expected from a given particle (π, K, p). The selection is expressed in units of the estimated resolution $\sigma_{\rm TOF}$ for each track, which has a mean value of 160 ps and 85 ps in pp and Pb–Pb collisions, respectively. The TOF allows pions and kaons to be unambiguously identified up to $p \sim$ 1.5-2.0 GeV/c. The two mesons can be distinguished from (anti)protons up to $p \sim$ 2.5 GeV/c. For the analyses described in this paper the start time of the collision (event time zero) is measured by the T0 detector, an array of Cherenkov counters located at +350 cm and -70 cm along the beam line. For events in which the T0 signal is not present, it is estimated using the particle arrival times at the TOF or the averaged collision time observed in the fill.

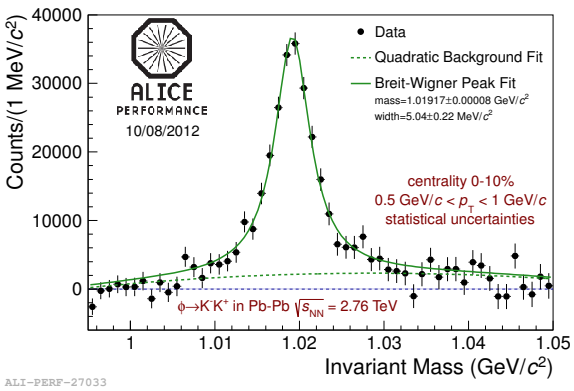

Figure 1. The K^+K^- invariant mass distribution in Pb–Pb collisions at $\sqrt{s_{NN}}$=2.76 TeV. The fitting function is the sum of a Breit-Wigner function and a polynomial.

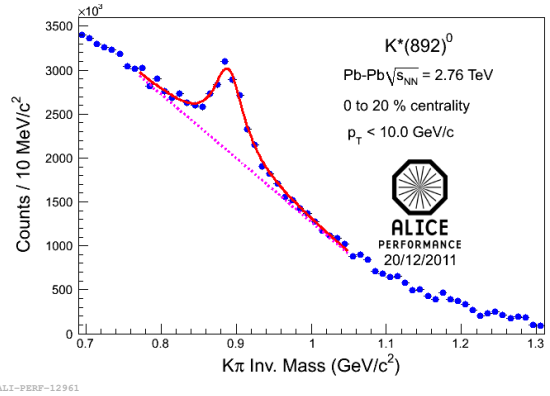

Figure 2. The $K\pi$ invariant mass distribution in Pb–Pb collisions at $\sqrt{s_{NN}}$=2.76 TeV. The fitting function is the sum of a Breit-Wigner function and a polynomial.

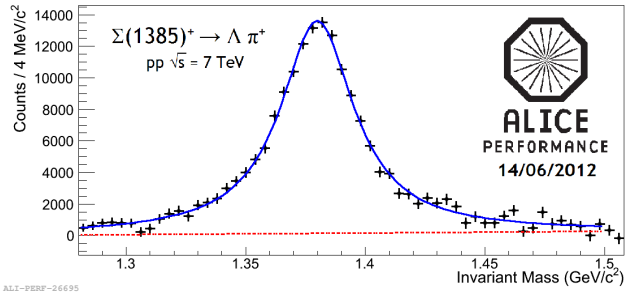

Figure 3. The $\Lambda\pi^+$ invariant mass distribution in pp collisions at $\sqrt{s}$=7 TeV after background subtraction. The solid line is the result of the combined fit: a Breit-Wigner function plus a polynomial. The dashed line describes the residual background.

2.2. Raw yield extraction and p_T spectrum

Resonances are identified by their main hadronic decay ($K^* \longrightarrow \pi^{\pm}+K^{\mp}$, $\phi \longrightarrow K^+ + K^-$, $\Sigma^{*\pm} \longrightarrow \Lambda\pi^{\pm}$). Due to their very short lifetimes, decay products cannot be distinguished from particles coming from the primary vertex. Their yield is obtained by computing the invariant mass spectrum of all primary candidates (tracks or hyperons) and then subtracting a combinatorial background. This was performed by the event-mixing or the like-sign technique. The signal, after subtracting the combinatorial background, was then fitted with a Breit-Wigner plus a polynomial for the residual background. A Voigtian function (convolution of Breit-Wigner function and Gaussian) was used in pp collisions for the extraction of the ϕ raw yield. For the Σ^*, the residual background originating from correlated $\Lambda\pi$ pairs coming from $\Lambda(1520)$ decay, has been estimated by Monte-Carlo simulations and subtracted before fitting the invariant mass spectrum. Some examples of invariant mass spectra are presented in Figs.1,2 and 3. The mass and width of analyzed resonances are close to the PDG values. In particular, in Pb-Pb collisions no mass shift nor broadening has been observed for the $\phi(1020)$, nor for $K^*(892)^0$, similar to what is observed in pp collisions.

In order to extract the total production yield, the raw counts were corrected for the decay branching ratio and for the losses due to geometrical acceptance and detector efficiency, which was determined by Monte-Carlo simulation using PYTHIA or HIJING generators, for pp and

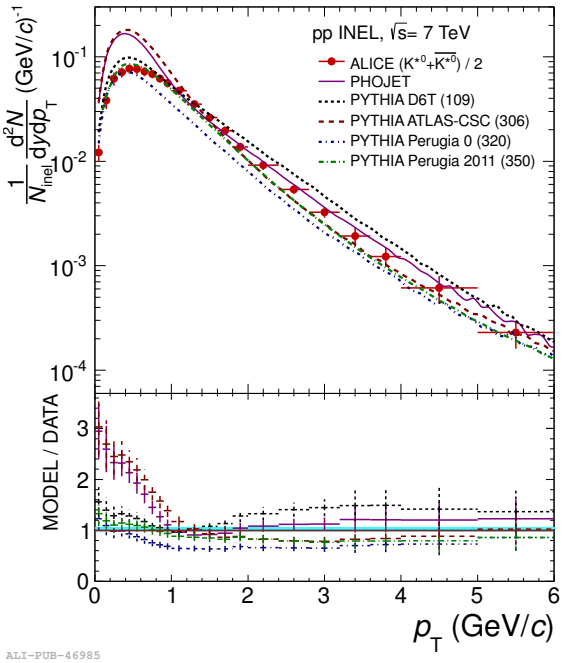

Figure 4. Comparison of the K* p_{T} spectrum in inelastic pp collisions at $\sqrt{s}$=7 TeV with PHOJET and PYTHIA tunes [15].

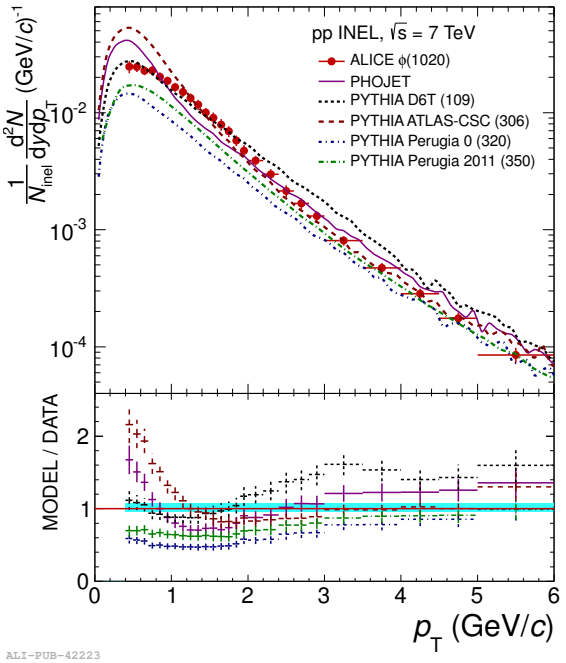

Figure 5. Comparison of the ϕ p_{T} spectrum in inelastic pp collisions at $\sqrt{s}$=7 TeV with PHOJET and PYTHIA tunes [15].

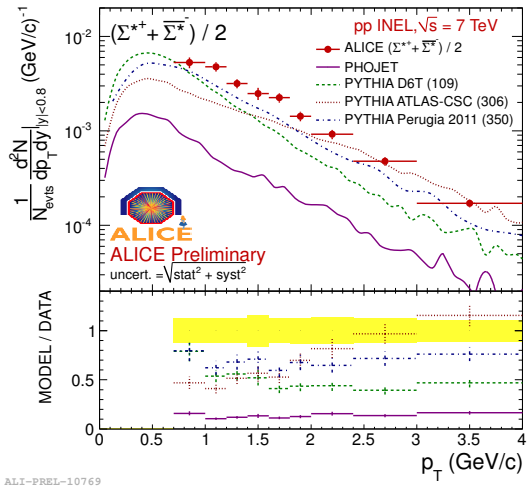

Figure 6. Comparison of the $(\Sigma^{*+} + \overline{\Sigma^{*-}})/2$ p_{T} spectrum in inelastic pp collisions at $\sqrt{s}$=7 TeV with PHOJET and PYTHIA tunes.

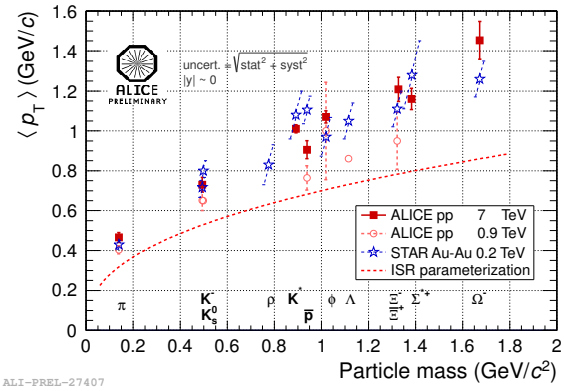

Figure 7. Mean transverse momentum $\langle p_{\mathrm{T}} \rangle$ as a function of the particle mass. Au-Au data at $\sqrt{s_{\mathrm{NN}}}$=0.2 TeV [22]; ALICE data for pp collisions at $\sqrt{s}$=0.9 TeV [23, 24]; ALICE data at $\sqrt{s}$=7 TeV [25].

Pb–Pb data, respectively. Final yields were obtained normalizing to the number of inelastic collisions (pp collisions) or to the number of analyzed events in a given centrality range (Pb–Pb collisions). The trigger efficiency was also taken into account. The analyses of K*(892)^0 and ϕ(1020) mesons in pp collisions at $\sqrt{s}$=7 TeV are described in detail in [15].

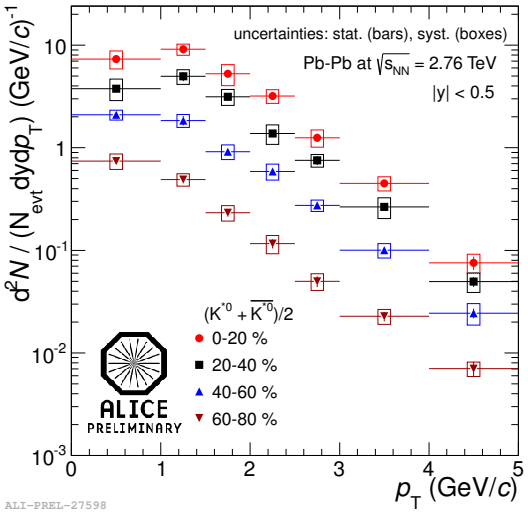

Figure 8. K* p_T spectra in Pb–Pb collisions at $\sqrt{s_{NN}}$=2.76 TeV at different centralities.

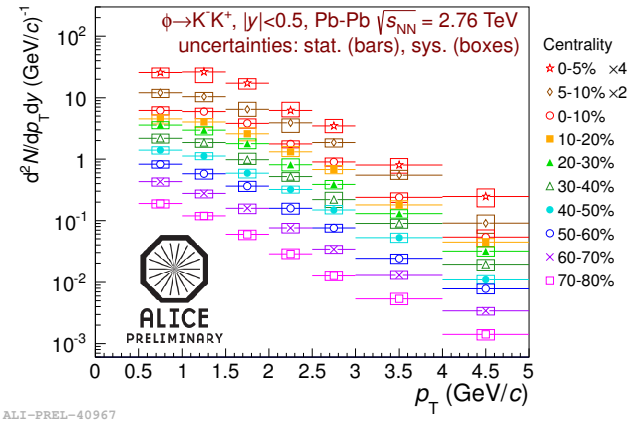

Figure 9. $\phi(1020)$ p_T spectra in Pb–Pb collisions at $\sqrt{s_{NN}}$=2.76 TeV at different centralities.

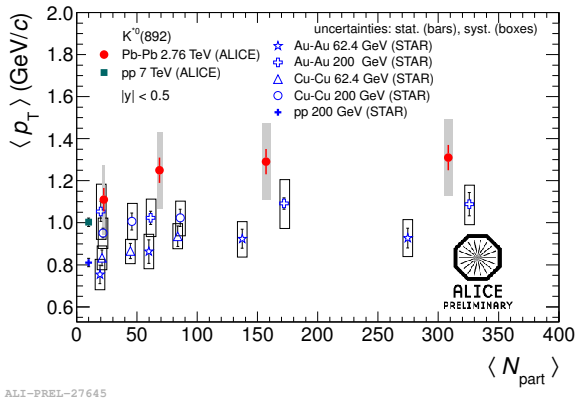

Figure 10. Mean transverse momentum of K* meson as a function of the mean number of participants for STAR [31] and ALICE data.

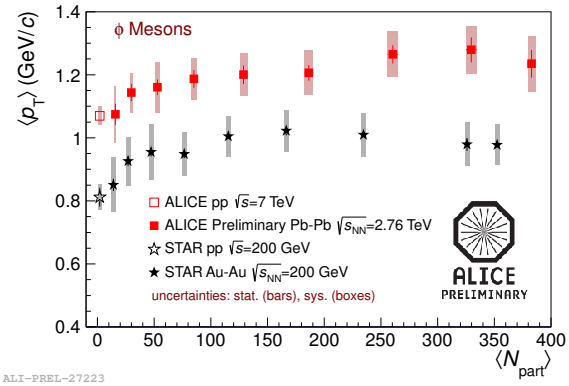

Figure 11. Mean transverse momentum of $\phi(1020)$ meson as a function of the mean number of participants for STAR [20, 28] and ALICE data [15].

3. Results

3.1. pp collisions at $\sqrt{s}$=7 TeV

Figures 4, 5 and 6 show the K* [1], $\phi(1020)$ and $(\Sigma^{*+} + \overline{\Sigma^{*+}})/2$ spectra with a comparison to a number of PYTHIA [16, 17, 18] tunes and PHOJET [3]. The best agreement is found for the recent PYTHIA Perugia 2011 tune. In fact there is a good agreement of the model to the data for the K*. It reproduces only the high p_T part (p_T>3 GeV/c) of the ϕ spectrum. Very poor agreement is found for the baryonic resonance.

The spectra have been fitted by a Tsallis function [19] and the extracted n values (6.2±0.07±0.8 and 6.7±0.20±0.4 for K* and ϕ, respectively) are similar to those quoted by the STAR experiment at RHIC for the ϕ measured in pp collisions at 200 GeV ($n = 8.3 \pm 1.2$) [20].

[1] We denote by K* the average of K^{*0} and $\overline{K^{*0}}$.

In contrast, the slope parameters (254±2±18 and 272±4±11 MeV for K* and ϕ, respectively) are significantly higher than the values obtained at RHIC, $T = 202 \pm 14 \pm 11$ MeV for ϕ [21]. For the ϕ the inelastic yield increases proportionally to the charged particle multiplicity from 0.9 to 7 TeV. The mean transverse momenta $\langle p_{\rm T} \rangle$ for K*, $\phi(1020)$ and $\Sigma(1385)^{\pm}$ are presented in Fig. 7 as a function of the particle mass. They follow the trend observed for stable particles indicating a common production mechanism. In this figure the $\langle p_{\rm T} \rangle$ for different system and various collision energies (ALICE pp data at 0.9 and 7 TeV, STAR Au-Au data at $\sqrt{s_{\rm NN}}$=0.2 TeV) are also shown.

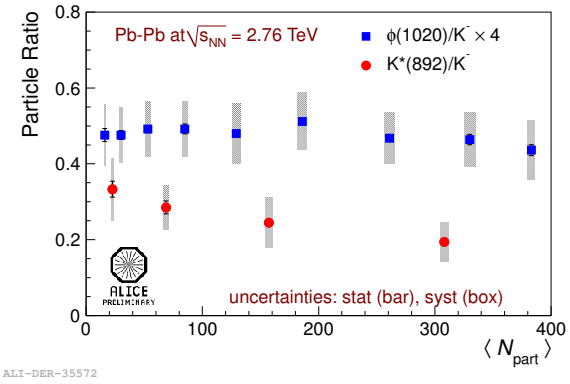

Figure 12. K*/K, ϕ/K ratios as a function of mean number of participants in Pb–Pb collisions at $\sqrt{s_{\rm NN}}$=2.76 TeV.

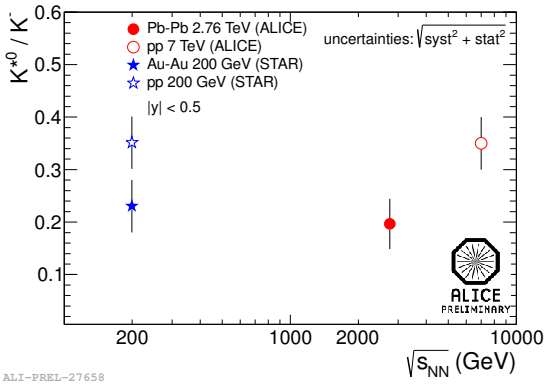

Figure 13. K*/K ratio as a function of the collision energy. Open symbols are for pp data, closed symbols for ion-ion data [31, 15].

3.2. Pb–Pb collisions at $\sqrt{s_{\rm NN}}$=2.76 TeV

The transverse momentum spectra for K* and ϕ in several event centrality bins are shown in Figs. 8 and 9. The mean transverse momentum as a function of the mean number of participant $\langle N_{\rm part} \rangle$ at LHC and at RHIC energies for K* and $\phi(1020)$ is shown in Figs. 10 and 11, respectively. We note that the $\langle p_{\rm T} \rangle$ measured in pp collisions at $\sqrt{s}$=7 TeV is equal to the value measured in Pb–Pb peripheral collisions at $\sqrt{s_{\rm NN}}$=2.76 TeV. For the ϕ, the $\langle p_{\rm T} \rangle$ at LHC energies is larger than the one at RHIC energies. This is consistent with a stronger radial flow at LHC than RHIC. In fact, a global blast-wave fit of π, K, p shows a 10% increase in $\langle \beta_{\rm T} \rangle$ with respect to RHIC [29], for central collisions.

In heavy ion collisions, the yields for stable and long-lived hadrons reflect the thermodynamic conditions (temperature, chemical potentials) at freeze-out, whereas the yield for short-lived resonances can be modified by final-state interactions inside the hot and dense reaction zone [5, 30]. Particularly interesting is the comparison of $\phi(1020)$ and K* production, considering the different lifetimes (about a factor of 10) of the two resonances.

While the ϕ/K ratio is independent of the collision centrality, the K*/K ratio decreases with increasing centrality (Fig.12). Figure 13 shows that the K*/K ratio in pp collisions is the same at RHIC and at the LHC. In contrast, this ratio decreases in heavy ion collisions and this effect seems to be larger at the LHC energies. The difference in K* and ϕ production could be related to the interaction of K* with hadronic medium, which does not affect the ϕ yield due to its long lifetime. Figure 14 shows the decrease of the K*/K ratio with respect to the system size represented by $({\rm d}N_{\rm ch}/{\rm d}\eta)^{1/3}$ for the different data sets of different collision systems and energies. The fact that they all fall on a common line could indicate that the observed decrease is related to the radial extent of the fireball. The decrease could be caused by the pion

rescattering mechanism ($\sigma(\pi,\pi)$), which destroyes the pion-kaon correlation of the K* decay products. However, there is also the possibility that the ratio K*/K changes from chemical to kinetic freeze-out just by the variation of the temperature.

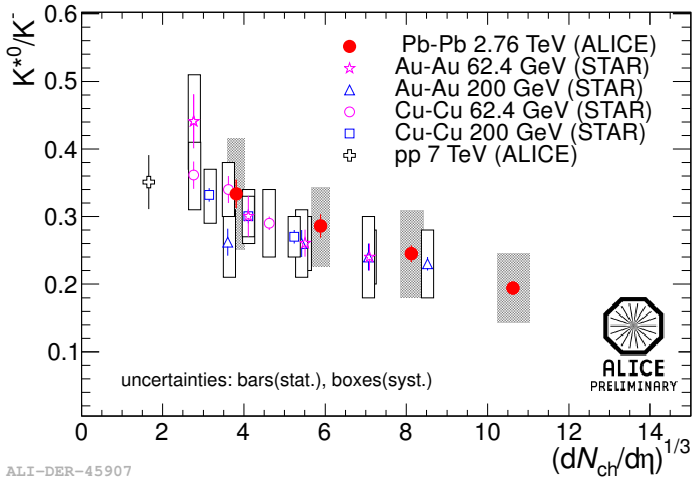

Figure 14. K*/K ratio as a function of $(\mathrm{d}N_{\mathrm{ch}}/\mathrm{d}\eta)^{1/3}$. STAR data are from [31].

4. Conclusions

The hadronic resonance $\mathrm{K}^*(892)^0$, $\phi(1020)$ and $\Sigma(1385)^{\pm}$ have been measured in pp collisions at $\sqrt{s}$=7 TeV and in Pb–Pb collisions at $\sqrt{s_{\mathrm{NN}}}$=2.76 TeV for different event centrality bins by the ALICE experiment at the LHC. Transverse momentum spectra of $\mathrm{K}^*(892)^0$, $\phi(1020)$ and $\Sigma(1385)^{\pm}$ measured in pp collisions have been compared to PHOJET and different PYTHIA tunes. Only the $\mathrm{K}^*(892)^0$ is reproduced by Perugia 2011 PYTHIA tune. None of tunes gives a satisfactory description of the $\phi(1020)$ and $\Sigma(1385)^{\pm}$ data.

In proton-proton collisions the mean transverse momenta increase with the collision energy and they follow the trend of the stable particles.

While the ϕ/K is rather flat versus centrality, the K*/K ratio decreases with centrality. It is shown that this decrease is related to the radial extension of the fireball.

References

[1] Aguilar-Benitez M et al. (LEBC-EHS Collaboration) 1991 Inclusive particle production in 400 GeV/c pp-interactions *Z. Phys.* C **50** 405
[2] Albrecht H et al. 1994 Inclusive production of K*(892), $\rho^0(770)$, and $\omega(780)$ mesons in the Υ energy region *Z. Phys.* C **61** 1
[3] Engel R 1995 Photoproduction within the two component dual parton model. Amplitudes and cross-sections *Z. Phys.* C **66** 203; Engel R and Ranft J 1996 Hadronic photon-photon interactions at high-energies *Phys. Rev.* D **54**, 4244.
[4] Sjöstrand T, Mrenna S and Skands P 2006 PYTHIA 6.4 physics and manual *J. High Energy Phys.* **05** 026
[5] Bleicher M and Aichelin J 2002 Strange resonance production: Probing chemical and thermal freezeout in relativistic heavy ion collisions *Phys. Lett.* B **530** 81
[6] Bleicher M and Stöcker H 2004 Dynamics and freeze-out of hadron resonances at RHIC *J. Phys. Nucl. Part. Phys.* G. **30** S111
[7] Markert C et al. 2002 Strange hadron resonances: freeze-out probes in heavy-ion collisions *Proceedings* of PASI 2002 and *hep-ph*/0206260
[8] Vogel S and Bleicher M 2005 Resonance absorption and regeneration in relativistic heavy ion collisions *Proceedings* of Nucl. Phys. Winter Meeting 2005 in Bormio and *nucl-th*/0505027v1

[9] Andronic A et al. 2009 Thermal hadron production in relativistic nuclear collisions: the hadron mass spectrum, the horn, and the QCD phase transition *Phys. Lett.* B **673** 142
[10] Andronic A et al. 2012 The statistical model in Pb-Pb collisions at the LHC *arXiv* 1210.7724v1
[11] Torrieri G and Rafelski J 2001 Strange hadron resonances as a signature of freeze-out dynamics *Phys. Lett.* B **509** 239
[12] Aamodt K et al. (ALICE Collaboration) 2008 The ALICE experiment at the CERN LHC *J. Instrum.* **3** S08002
[13] Aamodt K et al. (ALICE Collaboration) 2010 Alignment of the ALICE Inner Tracking System with cosmic-ray tracks *J. Instrum.* **5** P03003
[14] Alme J et al. 2010 The ALICE TPC, a large 3-dimensional tracking device with fast readout for ultra-high multiplicity events *Nucl. Instrum. Meth. in Phys. Res.* A **622** 316
[15] Abelev B et al. (ALICE Collaboration) 2012 Production of $K^*(892)^0$ and $\phi(1020)$ in pp collisions at $\sqrt{s}$=7 TeV *Eur. Phys. J.* C **72** 2183
[16] Field R 2008 Physics at the Tevatron *Acta Phys. Pol.* B **39** 2611; Field R 2008 Studying the underlying events at CDF and the LHC *Proceedings* of the First International Workshop on Multiple Partonic Interactions at the LHC, (MPI08), Perugia(Italy) 27-31 October(2008),pag. 12 *arXiv*:1003.4220
[17] Buttar C et al. 2004 Simulations of minimum bias events and the underlying event, MC tuning and predictions for the LHC *Acta Phys. Pol.* B **35** 433
[18] Skands P Z 2010 Tuning Monte Carlo Generators: The Perugia Tunes *Phys. Rev.* D **82** 074018
[19] Tsallis C 1988 Possible generalization of Boltzmann-Gibbs statistics *J. Stat. Phys.* **52** 479
[20] Abelev B I et al. (STAR Collaboration) 2009 Measurements of ϕ meson production in relativistic heavy-ion collisions in the BNL Relativistic Heavy Ion Collider (RHIC) *Phys. Rev.* C **79** 064903
[21] Adams J et al. (STAR Collaboration) 2005 $K(892)^*$ resonance production in Au+Au and p+p collisions at $\sqrt{s_{NN}}$=200 GeV *Phys. Rev.* C **71** 064902
[22] Abelev B I et al. (STAR Collaboration) 2007 Strange particle production in p+p collisions at $\sqrt{s}$= 200-GeV *Phys. Rev.* C **75** 064901
[23] Aamodt K et al. (ALICE Collaboration) 2011 Strange particle production in proton-proton collisions at $\sqrt{s}$=0.9 TeV with ALICE at the LHC *Eur. Phys. J.* C **71** 1594
[24] Aamodt K et al. (ALICE Collaboration) 2011 Production of pions, kaons and protons in pp collisions at $\sqrt{s}$=900 GeV with ALICE at the LHC *Eur. Phys. J.* C **71** 1655
[25] Abelev B et al. (STAR Collaboration) 2012 Multi-strange baryon production in pp collisions at $\sqrt{s}$=7 TeV with ALICE *Phys. Lett.* B **712** 309
[26] Abelev B et al. (STAR Collaboration) 2006 Strange baryon resonance production in $\sqrt{s_{\rm NN}}$=200 GeV p+p and Au+Au collisions *Phys. Rev. Lett.* **97** 132301
[27] Abelev B et al. (STAR Collaboration) 2009 Systematic measurements of identified particle spectra in pp, d+Au, and Au+Au collisions at the STAR detector *Phys. Rev.* C **79** 034909
[28] Adams J et al. (STAR Collaboration) 2005 ϕ meson production in Au+Au and p+p collisions at $\sqrt{s_{\rm NN}}$=200 GeV *Phys. Lett.* B **612** 181
[29] Abelev B et al. (ALICE Collaboration) 2012 Pion, kaon, and proton production in central Pb-Pb collisions at $\sqrt{s_{\rm NN}}$=2.76 TeV *Phys. Rev. Lett.* **109** 252301
[30] Markert C 2005 Resonance production in heavy ion collisions *J. Phys. Nucl. Part. Phys.* G **31** S897
[31] Aggarwal M M et al. (STAR Collaboration) 2011 K^{*0} production in Cu+Cu and Au+Au collisions at $\sqrt{s_{\rm NN}}$=62.4 GeV and 200 GeV *Phys. Rev.* C **84** 034909